Electronic states of thiophenyl and furanyl radicals and dissociation energy of thiophene via photoelectron imaging of negative ions

Lori Marie Culberson and Andrei Sanov[a)]
Department of Chemistry and Biochemistry, University of Arizona, Tucson, Arizona 85721, USA

(Received 29 March 2011; accepted 3 May 2011; published online 26 May 2011)

We report photoelectron images and spectra of deprotonated thiophene, $C_4H_3S^-$, obtained at 266, 355, and 390 nm. Photodetachment of the α isomer of the anion is observed, and the photoelectron bands are assigned to the ground X^2A' (σ) and excited A^2A'' and B^2A'' (π) states of the thiophenyl radical. The photoelectron angular distributions are consistent with photodetachment from the respective in-plane (σ) and out-of-plane (π^*) orbitals. The adiabatic electron affinity of α-$^\bullet C_4H_3S$ is determined to be 2.05 ± 0.08 eV, while the B^2A'' term energy is estimated at 1.6 ± 0.1 eV. Using the measured electron affinity and the electron affinity/acidity thermodynamic cycle, the C–H_α bond dissociation energy of thiophene is calculated as $DH_{298}(H_\alpha–C_4H_3S) = 115 \pm 3$ kcal/mol. Comparison of this value to other, previously reported C–H bond dissociation energies, in particular for benzene and furan, sheds light of the relative thermodynamic stabilities of the corresponding radicals. In addition, the 266 nm photoelectron image and spectrum of the furanide anion, $C_4H_3O^-$, reveal a previously unobserved vibrationally resolved band, assigned to the B^2A'' excited state of the furanyl radical, $^\bullet C_4H_3O$. The observed band origin corresponds to a 2.53 ± 0.01 eV B^2A'' term energy, while the resolved vibrational progression (853 ± 42 cm^{-1}) is assigned to an in-plane ring mode of α-$^\bullet C_4H_3O$ (B^2A''). © *2011 American Institute of Physics*. [doi:10.1063/1.3593275]

I. INTRODUCTION

As technological advancements turn toward organic systems, it becomes imperative to advance the understanding of the fundamental compounds from which these novel materials are built. Thiophene (C_4H_4S, shown in Fig. 1) and furan (C_4H_4O, structure similar to that of thiophene) are two simple organic compounds that stand as fundamental examples in the field of heterocyclic chemistry. For example, they are used as mediators in synthetic reactions, predominantly targeting functionalized materials,[1] and play important roles in the pyrolysis of fossil fuels.[2] Polythiophenes are electrically conductive polymers,[3] and thus thiophene derivatives, such as 3,3′-bis(3,5-di-*tert*-butyl-4-methoxyphenyl)-2,2′-bithiophene, have shown promise as high-endurance organic memory devices,[4] while furan polymers include a wide variety of structures important in vegetable renewable resources.[5]

The electronic and vibrational structures of furan and thiophene have been studied in detail by various methods[6–8] including angle and vibrationally resolved photoelectron spectroscopy.[9,10] The importance of these molecules in the areas of optoelectronic devices, conductivity, and photoconductivity,[11,12] as well as combustion and pyrolysis, stimulate interest also in the respective radical and anion species. The C–H bond cleavage in furan and thiophene yields the furanyl ($^\bullet C_4H_3O$) and thiophenyl ($^\bullet C_4H_3S$) radicals, respectively, while deprotonation results in the closed-shell furanide ($C_4H_3O^-$) and thiophenide ($C_4H_3S^-$) anions. The H/H^+ elimination/abstraction can occur either at the α or β position, giving rise to the respective α and β isomers of the corresponding radicals or anions. For thiophene, the structures and nomenclature for the closed-shell molecule, its radicals and anions (both α and β isomers) are shown in Fig. 1. Chemical intuition and theoretical modeling dictate that α is the more acidic center in both thiophene and furan, but DePuy *et al.* noted that β-hydrogens can also be abstracted in exchange reactions with deuterated alcohols.[13]

In this work, we focus primarily on photoelectron spectroscopy of the thiophenide anion, $C_4H_3S^-$. The process of photodetachment provides spectroscopic access[14] to the ground and excited states of the corresponding neutral radical, $^\bullet C_4H_3S$. The past investigations of thiophene, as well as (until recently) furan, focused on the neutral molecules and their cations, while the anions had received no attention. However, as this work was being prepared for publication, a photoelectron spectroscopic study of the furanide anion was reported by Lineberger *et al.*[15] The photoelectron spectrum of $C_4H_3O^-$ revealed the presence of only the α isomer. The measured adiabatic electron affinity (EA) of α-$^\bullet C_4H_3O$, 1.854 ± 0.004 eV, combined with the known gas-phase acidity of furan, allowed the determination of the C–H_α bond dissociation energy of furan, $DH_{298}(H_\alpha – C_4H_3O) = 119.8 \pm 0.2$ kcal/mol.[15]

The relative energetics of the α and β isomers of $C_4H_3S^-$, as well as the corresponding neutral radicals, is indicated in Fig. 1. In what follows, we present the photoelectron images of $C_4H_3S^-$ obtained at 266, 355, and 390 nm. In the photodetachment of the anion, we access the X^2A' ground state as well as the A^2A'' and B^2A'' excited electronic states of the neutral radical. From the measured electron affinity and known gas-phase acidity of thiophene, we calculate the C–H_α bond dissociation energy of this important aromatic

a)Electronic mail: sanov@u.arizona.edu.

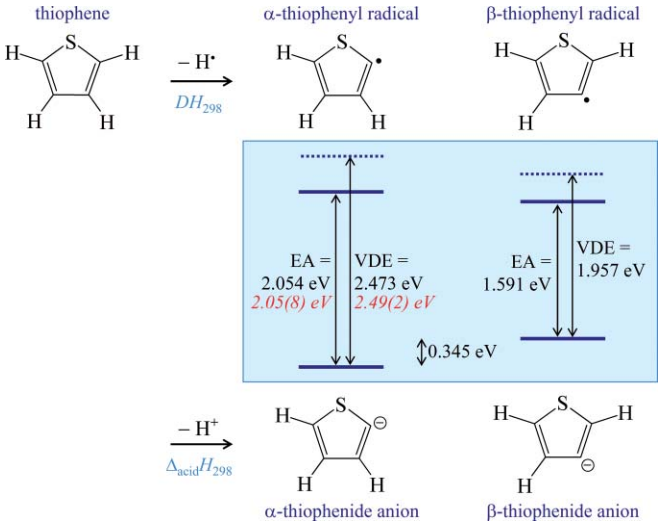

FIG. 1. Possible isomers resulting from the C–H bond dissociation and deprotonation of thiophene. The energetic values shown in black (roman type) are calculated at the UB3LYP/aug-cc-pVDZ level of theory, while those in red (italics) are determined experimentally in this work.

hydrocarbon and compare it to furan,[15] shedding light on substitution effects in heterocyclic chemistry. In addition, we present a 266 nm photoelectron image and spectrum of the furanide anion, extending the Lineberger *et al.*'s study[15] to higher binding energies. Our spectrum reveals an additional vibrationally resolved band assigned to the previously unobserved B^2A'' excited state of $^{\bullet}C_4H_3O$.

II. EXPERIMENTAL AND THEORETICAL METHODS

The experiments were performed using a negative-ion photoelectron imaging spectrometer that has been described in detail previously.[16] In brief, the instrument consists of a pulsed ion source, a time-of-flight mass spectrometer,[17] and a velocity-map[18] photoelectron imaging[19,20] assembly. Room-temperature thiophene or furan vapors, seeded in Ar carrier gas, were introduced into a high-vacuum chamber through a pulsed supersonic nozzle (General Valve Inc., Series 9), operating at a 50 Hz repetition rate and a 25 psi backing pressure. Anions were formed[21] via secondary-electron attachment following bombardment of the supersonic expansion of the precursor gas mixture with high-energy (1 keV) electrons from a custom-built continuous-beam electron gun. The anions were extracted into a Wiley–McLaren[22] time-of-flight mass spectrometer, where they were further accelerated to ~2.5 keV, focused with an Einzel lens, and detected with a dual-microchannel plate (MCP) detector. In the velocity-map imaging region, the ion beam was crossed (at a right angle) with a linearly polarized pulsed laser beam, timed to overlap only with the ions of interest. In this work, we used the frequency tripled (355 nm) or quadrupled (266 nm) output from a pulsed Nd:YAG (yttrium aluminum garnet) laser (Spectra Physics, Inc., Lab-50 model with pulse energies 3.5 and 0.07 mJ, respectively). The 390 nm radiation (0.2 mJ, 100 fs pulses) was generated as the second harmonic of an amplified Ti:sapphire laser system (Spectra Physics, Inc.).

The velocity-map imaging assembly is principally based on the original design by Eppink and Parker.[18] The laser polarization axis was set parallel to the plane of the imaging detector. An electrostatic lens mapped the photodetached electrons onto a position sensitive MCP detector fiber-optically coupled to a P47 phosphor screen (Burle, Inc.). A digital charge-coupled device camera recorded the electron impacts appearing on the phosphor screen. Each of the photoelectron images reported here represents $\sim 10^5$ experimental cycles. The three-dimensional probability distributions were reconstructed from the raw images via inverse Abel transformation[20] using the basis set expansion method and program.[23] Photoelectron images of I^- were used to calibrate the electron kinetic energy (eKE) scale of all reported images. Each photoelectron spectrum was fit to a sum of Gaussian functions, and angular distributions were calculated over the full width at half maximum of each transition. The experimentally determined angular distributions were analyzed using the standard procedure[20,23] to determine the values of the photoelectron anisotropy parameter β.[24,25]

Density-functional theory (DFT) calculations were carried out at the UB3LYP/aug-cc-pVDZ level using the GAUSSIAN 09 software package.[26] Geometry optimizations and harmonic vibrational frequencies were calculated for the ground states of each anion studied and its corresponding neutral. Energies were also computed for the neutral fixed at the equilibrium geometry of the corresponding anion.

III. RESULTS

The experimental results for the thiophenide anion, $C_4H_3S^-$, are displayed in Fig. 2. The photoelectron images, obtained at (a) 266, (b) 355, and (c) 390 nm, are shown on the left, the corresponding Abel inversions on the right, while the photoelectron spectra are in the middle. The furanide anion, $C_4H_3O^-$, was also studied at 266, 355, and 390 nm. The 355 and 390 nm results are consistent with the Lineberger *et al.*'s 364 nm study[15] and are not included here. The 266 nm image revealed a previously unobserved electronic state of the $^{\bullet}C_4H_3O$ radical, and these results are presented in Fig. 3. For direct comparison of the data collected at different laser wavelengths, all spectra in Figs. 2(a)–2(c) and 3 are plotted versus electron binding energy, eBE = $h\nu$ − eKE.

The lowest-eBE bands in Figs. 2(a)–2(c) and 3 are labeled X. They result from removal of an electron from the highest-occupied molecular orbital (HOMO) of the anion, to form the ground electronic state of the corresponding neutral radical. Transitions A and B are assigned to excited electronic states of the neutral radicals. Despite the significant overlap between bands X and A of both $C_4H_3S^-$ and $C_4H_3O^-$, the two transitions are clearly resolved by eye in the 266 nm photoelectron images (Abel-inverted, in particular), aided by the differing photoelectron angular distributions.

The vertical detachment energies (VDE), determined as the binding energies corresponding to band maxima, are summarized in Table I, along with the estimated band origins (eBE_0), photoelectron anisotropy parameter values (266 nm only), and state assignments. In addition, Table II summarizes the experimentally determined adiabatic electron affinities

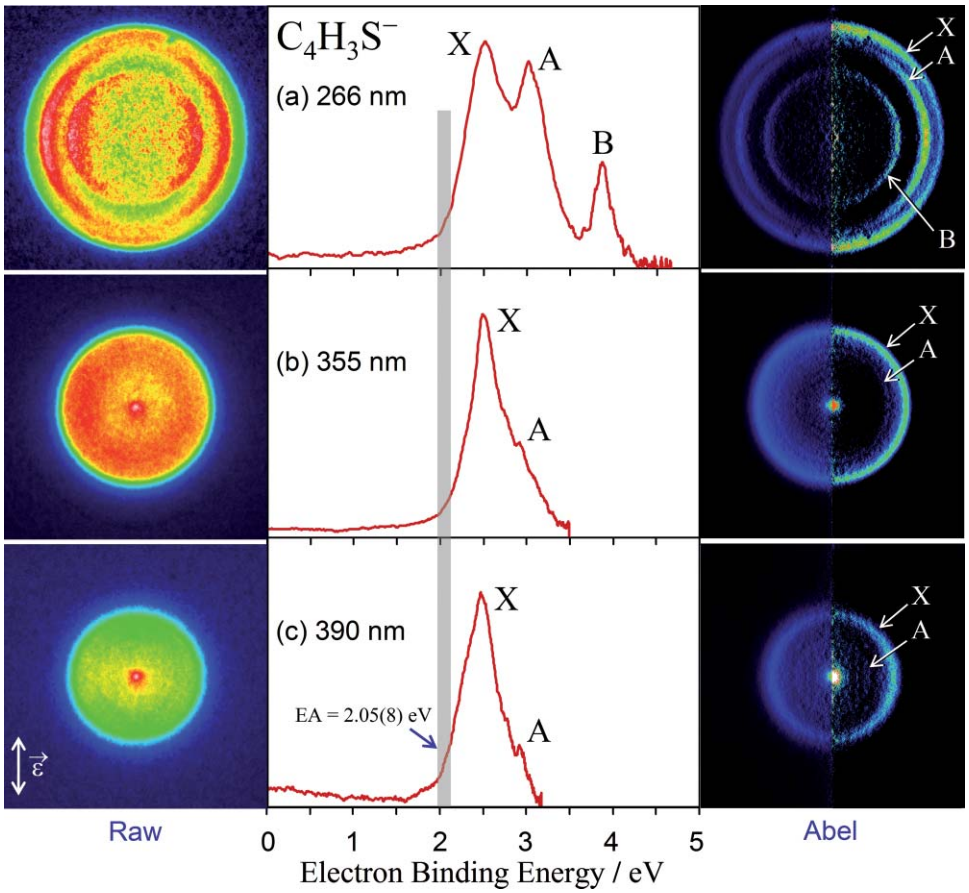

FIG. 2. Raw (left) and Abel-inverted (right) photoelectron images and corresponding spectra (center) for thiophenide obtained at (a) 266, (b) 355, and (c) 390 nm. The Abel-inverted images are displayed in split scale, in order to highlight the various-intensity transitions observed in the images; the left and right halves correspond to the same data normalized to different maximum intensities. The laser polarization axis is vertical in the plane of the figure, as indicated by the double arrow in the bottom left corner. The grey vertical stripe indicates the confidence interval for the X band origin.

and excited-state term energies of the α-thiophenyl and α-furanyl radicals. Without vibrational resolution, determination of band origins and, therefore, electron affinities presents a challenge, resulting in significant uncertainty limits. The confidence interval for the X band origin in $C_4H_3S^-$ is indicated in the spectra in Fig. 2(a)–2(c) with a grey vertical stripe. The corresponding energy range is assigned as adiabatic electron affinity of the thiophenyl radical, EA($^\bullet C_4H_3S$) = 2.05 ± 0.08 eV. This assignment is in excellent agreement with the predicted EA(α-$^\bullet C_4H_3S$) = 2.054 eV obtained at the UB3LYP/aug-cc-pVDZ level of theory. Similar analysis of our furanide spectra, including the 266 nm results (Fig. 3) and the 355 and 390 nm data (not shown), yields EA($^\bullet C_4H_3O$) = 1.84 ± 0.07 eV, as indicated by a grey vertical stripe in Fig. 3. This determination is in agreement with the higher resolution measurement of 1.853 ± 0.004 eV.[15] The agreement boosts our confidence in the EA of thiophenyl radical, as it was obtained using the same procedure.

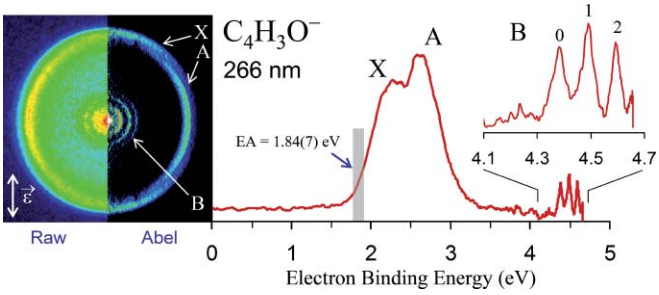

FIG. 3. Raw (left) and Abel-inverted (right) photoelectron images and corresponding spectrum (far right) of furanide obtained at 266 nm. The laser polarization axis is vertical in the plane of the figure. Band B is expanded as an inset, and the grey vertical stripe indicates the confidence interval for the X band origin.

The three measurements of band X's maximum (266, 390, and 355 nm spectra in Fig. 2 and Table I) yield the vertical detachment energy of $C_4H_3S^-$, VDE = 2.49 ± 0.02 eV. The 390 and 355 nm spectra each reveal a shoulder, marked A, on the high eBE side of band X. The additional transition is more apparent in the angle-resolved images, rather than the integrated spectra, due to the differing anisotropy properties of bands A and X. The low intensity of band A (relative to X) at 390 and 355 nm may be, in part, due to the low eKE associated with this band at these wavelengths, resulting in a Wigner-like centrifugal-barrier suppression of the photodetachment cross sections.[27,28] Accordingly, transition A is best seen in the higher photon energy 266 nm image/spectrum in Fig. 2(a). The origin of this transition in not resolved because of the overlap with band X. The 266 nm photoelectron image of $C_4H_3S^-$ also reveals another higher energy band, B, with a

TABLE I. $C_4H_3S^-$ and $C_4H_3O^-$ photoelectron spectral features observed in this work at the wavelengths indicated (nm), including band origins and peak binding energies (both in electron volts), anisotropy parameters (β), and neutral state assignments.

Band		Peak eBE/ VDE	Band origin, eBE_0/EA	β	Neutral radical state assignment
$C_4H_3S^-$					
X	266	2.49 ± 0.04	2.05 ± 0.08 [a]	0.27 ± 0.01	$X\,^2A'$
	355	2.50 ± 0.03			
	390	2.47 ± 0.03			
A	266	3.05 ± 0.04		-0.38 ± 0.02	$A\,^2A''$
B	266	3.86 ± 0.03	3.64 ± 0.05	-0.40 ± 0.04	B^2A''
$C_4H_3O^-$					
X	266	2.14 ± 0.04	1.84 ± 0.07 [a]	0.47 ± 0.01	$X\,^2A'$
A	266	2.63 ± 0.04		-0.34 ± 0.01	$A\,^2A''$
B: B_0	266	4.38 ± 0.01	4.38 ± 0.01 [b]	-0.51 ± 0.04	$B\,^2A''$
B_1	266	4.49 ± 0.01		-0.37 ± 0.04	
B_2	266	4.59 ± 0.01		-0.36 ± 0.02	

[a]Determined from combined analysis of the data obtained at all wavelengths studied (see text for details).
[b]Peak B_0 is assigned as band B origin.

maximum at VDE = 3.86 ± 0.03 eV, apparent origin at eBE_0 = 3.64 ± 0.05 eV, and an angular distribution peaking in the perpendicular direction.

Bands X and A in the 266 nm photoelectron image and spectrum of $C_4H_3O^-$ (Fig. 3) have been characterized previously by Vogelhuber *et al.*[15] Similar to $C_4H_3S^-$, the 266 nm photoelectron angular distributions for band X and A peak in the directions parallel and perpendicular to the laser polarization axis, respectively (Table I). The peak position of band X in our spectrum, 2.14 ± 0.04 eV, is assigned as the VDE of $C_4H_3O^-$. This result is consistent with the vibrationally resolved spectrum.[15]

In addition, the 266 nm photoelectron image of $C_4H_3O^-$ exhibits a series of rings near the center, corresponding to the onset of another, vibrationally resolved electronic transition (B). This transition is above the energetic cutoff of the previous measurement.[15] The corresponding spectrum reveals well-resolved vibrational structure, with an average spacing of 853 ± 42 cm^{-1}. The first peak (B_0), corresponding to the transition origin, is centered at eBE = 4.38 ± 0.01 eV, which is assigned as the electron affinity (i.e., adiabatic binding energy) of the second excited state of the $^{\bullet}C_4H_3O$ radical. The photoelectron angular distribution, corresponding to band B, peaks in the direction perpendicular to the laser polarization axis (see Table I).

TABLE II. Electron affinities and excited-state term energies (T_e) of the thiophenyl and furanyl radicals (in electron volts).

	α-thiophenyl	α-furanyl
EA ($X\,^2A'$)	2.05 ± 0.08[a]	1.84 ± 0.07[a]
		1.853 ± 0.004[b]
T_e ($A\,^2A''$)	~0.6[a,c]	0.68 ± 0.07[b]
T_e($B\,^2A''$)	1.6 ± 0.1[a]	2.53 ± 0.01[a,d]

[a]This work.
[b]Reference 15.
[c]Crude estimate based on the difference in the VDEs of the $A\,^2A''$ and $X\,^2A'$ photodetachment transitions.
[d]Calculated as the difference between the eBE_0 reported in Table I and the EA value reported in Ref. 15.

IV. DISCUSSION

A. Electronic states of thiophenyl and furanyl radicals

The thiophenide and furanide anions and the corresponding neutral radicals have some common characteristics. The anions are closed-shell species, resulting from deprotonation of the respective thiophene and furan molecules. The ground electronic states of the corresponding neutral radicals, X^2A', are formed by ejecting one of the in-plane (a') HOMO electrons and can, therefore, be described as σ radicals. The two lowest excited neutral states, A^2A'' and B^2A'', result from electron detachment from one of the non-degenerate π^* orbitals of the anions, HOMO–1 and HOMO–2. These states are best thought of as π radicals.

The structural features of the thiophenide anion and thiophenyl radical were examined using DFT. After structure optimization at the UB3LYP/aug-cc-pVDZ level of theory, the α-$C_4H_3S^-$ isomer was found to be lower in energy by 0.345 eV relative to β-$C_4H_3S^-$ (not including the zero-point vibrational energy corrections), as indicated in Fig. 1. This energy gap is larger than that for the furanide anion, as similar calculations show α-$C_4H_3O^-$ to be 0.215 eV more stable than β-$C_4H_3O^-$. Photoelectron spectroscopy of the furanide anion revealed contributions from α-$C_4H_3O^-$ only, with no evidence for the higher energy β species.[15] Based on the relative energetics, isomer coexistence should be even less likely in $C_4H_3S^-$. Therefore, the results in Fig. 2 are attributed to the

photodetachment of more stable α-$C_4H_3S^-$. Similarly, the results in Fig. 3 are ascribed to the α form of $C_4H_3O^-$.

Photoelectron angular distributions reflect the properties of the parent orbital from which the electrons are detached and qualitative insight can often be gained through symmetry-based considerations.[16,29] Given the low symmetry of the furanide and thiophenide anions (C_s point group for both the α and β structures), predominantly parallel angular distributions ($\beta > 0$) are likely to arise in detachment from totally symmetric a' orbitals, while predominantly perpendicular PADs ($\beta < 0$) are generally expected in detachment from a'' orbitals.[16,30]

For reference, isosurface plots representing the in-plane σ (a') HOMO and out-of-plane π (a'') HOMO–1 and HOMO–2 for α-$C_4H_3S^-$ and α-$C_4H_3O^-$ are shown in Fig. 4. A similar qualitative depiction of the HOMO and HOMO–1 of α-$C_4H_3O^-$ is given in Ref. 15. The orbital symmetries, in conjunction with the experimentally determined anisotropy (β) values, aid in assignment of the features in the photoelectron spectra. In Table I, we report the 266 nm β values, which allow the comparison of all three photodetachment transition for each $C_4H_3S^-$ and $C_4H_3O^-$. Band X in $C_4H_3S^-$ exhibits a predominantly parallel photoelectron angular distribution, attributed to detachment from an a' orbital. This is consistent with the predicted symmetry of the $C_4H_3S^-$ HOMO (Fig. 4). Therefore, band X is assigned to the X^2A' state of the thiophenyl radical, $^\bullet C_4H_3S$, while the transition energy, 2.49 ± 0.02 eV, is assigned as the VDE of $C_4H_3S^-$. We note, however, that photoelectron anisotropy exhibits energy dependence, as usual in negative-ion photodetachment. In fact, examination of the images in Fig. 2 reveals that β for the X band changes sign from negative to positive, as photon energy and, therefore, eKE increase.

Bands A and B in $C_4H_3S^-$ exhibit predominantly perpendicular photoelectron angular distributions, suggesting detachment from an a'' orbital. This assignment is consistent with the predicted out-of-plane π character of the $C_4H_3S^-$ HOMO–1 and HOMO–2 (Fig. 4). We further note that these orbitals have significant character of an (atomic) d_{xy} orbital. This is particularly clear when the orbitals are considered from an outside viewpoint within the plane of the molecule, as shown in Fig. 4, column (b). Detachment from a *d*-like molecular orbital at moderate eKEs is known to yield predominantly perpendicular photoelectron angular distributions, as in the well studied cases of π_g^* photodetachment from O_2^- and S_2^-.[16,31–34] (Although the *gerade* symmetry is only approximate in the present case, the isosurface plots of $C_4H_3S^-$ HOMO–1 and HOMO–2, as rendered in Fig. 4(a), are quite reminiscent of the π_g^* HOMO of O_2^-.) Thus, we assign the A and B bands in Fig. 2 to the A^2A'' and B^2A'' states of $^\bullet C_4H_3S$, respectively. The energetic onset of band A in the $C_4H_3S^-$ photoelectron spectrum (Fig. 2) cannot be determined because of the overlap with band X, but a crude estimate of the A^2A'' term energy can be obtained from the VDE difference between bands A and X (Table II). The origin of band B, on the other hand, is quite clear at 3.64 ± 0.05 eV (Fig. 2 and Table I), corresponding to a $T_e(B^2A'') = 1.6 \pm 0.1$ eV term energy (Table II).

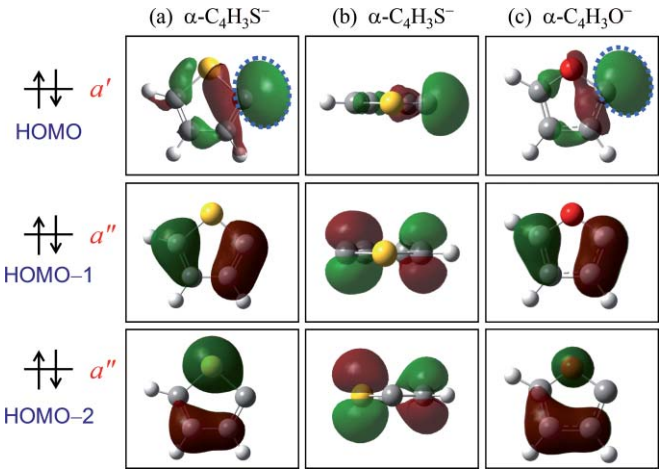

FIG. 4. Isosurface plots of the HOMO, HOMO–1, and HOMO–2 of α-thiophenide (columns a and b) and α-furanide (column c) anions, as determined at the uB3LYP/aug-cc-pVDZ level of theory. Columns (a) and (c) depict the α-$C_4H_3S^-$ and α-$C_4H_3O^-$ orbitals viewed from above the respective molecular planes, while column (b) shows the same α-$C_4H_3S^-$ orbitals viewed from within the molecular plane (note the different orientations of the anion within the plane in the three cases). The relative isosurface amplitudes [0.4 for $C_4H_3S^-$ in (a) and (b) versus 0.5 for $C_4H_3O^-$ in (c)] are chosen so that the C_α lone-pair components of the two HOMOs appear similar in size. To help guide the eye, the blue dashed lines drawn in (a) and (c) on top of the $C_4H_3S^-$ and $C_4H_3O^-$ lone-pair lobes of the respective HOMOs represent identical oval shapes). Inspection of the two HOMOs reveals a slightly greater degree of orbital delocalization in the $C_4H_3S^-$ case.

Similarly, band X in $C_4H_3O^-$ displays a predominantly parallel angular distribution, while band A peaks in the perpendicular direction (Fig. 3 and Table I). Consistent with the above discussion of $C_4H_3S^-$ and in agreement with the Lineberger *et al.*'s study of $C_4H_3O^-$,[15] these bands are assigned to the X^2A' and A^2A'' states of $^\bullet C_4H_3O$.

Band B in the $C_4H_3O^-$ spectrum has not been observed previously. From its origin, B_0 at eBE = 4.38 ± 0.01 eV (Table I) and the previously determined ground-state electron affinity, EA($^\bullet C_4H_3O$) = 1.853 ± 0.004 eV,[15] we determine the B^2A'' state term energy for $^\bullet C_4H_3O$, $T_e(B^2A'') = 2.53 \pm 0.01$ eV. The band exhibits vibrational structure with an average spacing of 853 ± 42 cm^{-1}. For comparison, Lineberger *et al.* observed a 855 ± 25 cm^{-1} vibrational mode, described as O–C–C bend, in $C_4H_3O^-$ photodetachment to the ground electronic state of $^\bullet C_4H_3O$.[15] Lineberger's B3LYP/6–311++G(d,p) and our B3LYP/aug-cc-pVDZ calculations indicate that this in-plane ground-state ring mode has a frequency of 868 cm^{-1}, while calculations on the A^2A'' excited state of the radical give a similar frequency, 866 cm^{-1}.[15] Although we did not carry out frequency calculations for the B^2A'' state of $^\bullet C_4H_3O$, we expect the results for the mode in question to be similar, because the second excited state is also π-radical in nature. In addition, Yang *et al.* observed a vibrational progression of the cation of furan, $C_4H_4O^+$, at 886 ± 5 cm^{-1} and assigned it to an in-plane ring vibrational mode of a_1 symmetry.[10] All of the above frequencies are in excellent agreement with band B's observed spectral interval. We thus assign the observed progression to this ring mode.

The photoelectron anisotropy values for the individual vibrational peaks of band B in $C_4H_3O^-$ are similar to the β

value for the corresponding band B in $C_4H_3S^-$ (see Table I). This is not surprising in view of the similarity of the respective detachment orbitals, HOMO–2 of $C_4H_3O^-$ and $C_4H_3S^-$ (see Fig. 4).

B. The C–H bond dissociation energy of thiophene

The experimentally determined adiabatic electron affinity of α-$^\bullet C_4H_3S$ allows us to calculate the C–H_α bond dissociation enthalpy, $DH_{298}(H_\alpha - C_4H_3S)$, of thiophene. This is done using the general acidity/electron affinity cycle,[35]

$$DH_{298}(R-H) = \Delta_{acid}H_{298}(RH) + EA(R^\bullet) - IE(H) + [\text{thermal correction}], \quad (1)$$

where $\Delta_{acid}H_{298}(RH)$ is the gas-phase acidity of a closed-shell molecule, $EA(R^\bullet)$ is the electron affinity of the corresponding radical, and IE(H) is the ionization energy of atomic hydrogen (13.60 eV = 313.6 kcal/mol).[36] The [thermal correction] term is an integral over changes in heat capacity. It is typically small (< 0.3 kcal/mol) (Ref. 37) and will be neglected in our calculations from here on. Substituting the previously measured gas-phase acidity of thiophene (α-position), $\Delta_{acid}H_{298}(C_4H_4S) = 381 \pm 3$ kcal/mol,[13] and the electron affinity of α-$^\bullet C_4H_3S$ determined here, $EA(^\bullet C_4H_3S) = 47.3 \pm 1.8$ kcal/mol (2.05 ± 0.08 eV), into Eq. (1), we calculate $DH_{298}(H_\alpha–C_4H_3S) = 115 \pm 3$ kcal/mol.

The main contribution to the large uncertainty of the above DH_{298} value comes from the uncertainty of the 1988 measurement of the acidity of thiophene (±3 kcal/mol), and not the photoelectron spectroscopic measurements (±1.8 kcal/mol). In fact, when the two above absolute uncertainties are combined (as square-root of sum squares), the result rounds off to the same value as the uncertainty of $\Delta_{acid}H_{298}(C_4H_4S)$. Therefore, for an improved determination of the C–H_α bond dissociation energy of thiophene via this method, it is imperative to have a more precise measurement of this molecule's acidity, as increasing the resolution of the anion's photoelectron spectroscopy alone will not affect the above error bars.

To emphasize this point, we turn to furan, for which gas-phase acidity was measured more recently, with greater precision than for thiophene: $\Delta_{acid}H_{298}(C_4H_4O) = 390.7 \pm 0.2$ kcal/mol.[38] Substituting this value and $EA(\alpha$-$^\bullet C_4H_3O) = 42.4 \pm 1.6$ kcal/mol (1.84 ± 0.07 eV), as determined here, into Eq. (1), we find $DH_{298}(H_\alpha–C_4H_3O) = 119.5 \pm 1.6$ kcal/mol. This result is in excellent agreement with the determination by Vogelhuber *et al.*, $DH_{298}(H_\alpha–C_4H_3O) = 119.8 \pm 0.2$ kcal/mol.[15] In this case, the higher resolution of Vogelhuber *et al.*'s photoelectron measurement yield a smaller uncertainty for the overall result.

Within the uncertainty limits, the C–H_α bond dissociation energy of thiophene (115 ± 3 kcal/mol, as determined here) is intermediate between that of furan (119.8 ± 0.2 kcal/mol) (Ref. 15) and benzene (112.9 ± 0.5 kcal/mol).[35,39] The higher bond dissociation energy of furan reflects thermodynamic instability of the furanyl radical compared, for example, to $^\bullet C_6H_5$.[15] The relative instability of $^\bullet C_4H_3O$ has been attributed to the near localization of the unpaired electron on the $^\bullet C_\alpha$ center.[15,40] The above bond dissociation energies suggest that the thiophenyl radical is slightly more stable, compared to furanyl, presumably because of greater delocalization of the unpaired electron in thiophenyl. Visual inspection of the thiophenide HOMO in Fig. 4 supports this observation, as the orbital density does appear to be more delocalized than in the furanide case.[41] Formation of the thiophenyl and furanyl radicals from the respective anions involves the removal of one of the HOMO electrons, leaving the other unpaired. Therefore, qualitatively, Fig. 4 suggests a greater degree of the unpaired electron delocalization in thiophenyl, compared to furanyl. This, in turn, translates into a smaller C–H_α bond-dissociation energy of thiophene, compared to furan.

V. CONCLUSIONS

The observed photoelectron images and spectra of $C_4H_3S^-$ are attributed to the photodetachment of the α isomer of the anion. The observed bands correspond to the ground σ-radical (X^2A') and the low-lying excited π-radical (A^2A'' and B^2A'') states of thiophenyl radical. The photoelectron angular distributions are consistent with photodetachment from the respective in-plane (σ) and out-of-plane (π^*) orbitals. The adiabatic electron affinity of α-$^\bullet C_4H_3S$ is determined to be 2.05 ± 0.08 eV, while the second excited state term energy is $T_e(B^2A'') = 1.6 \pm 0.1$ eV. Using the measured electron affinity and the affinity/acidity thermodynamic cycle, the C–H_α bond dissociation energy thiophene is determined, $DH_{298}(H_\alpha–C_4H_3S) = 115 \pm 3$ kcal/mol. This value is intermediate between the corresponding bond energies of furan (119.8 ± 0.2 kcal/mol) (Ref. 15) and benzene (112.9 ± 0.5 kcal/mol),[35] indicating that the α-thiophenyl radical is thermodynamically more stable than α-furanyl, but still less stable than $^\bullet C_6H_5$. The 266 nm photoelectron image and spectrum of $C_4H_3O^-$ reveals a vibrational progression (853 ± 42 cm^{-1}) assigned to an in-plane ring vibrational mode of the previously unobserved B^2A'' excited state of $^\bullet C_4H_3O$. The origin of this state is observed at 4.38 ± 0.01 eV, corresponding to an electronic term energy $T_e(B^2A'') = 2.53 \pm 0.01$ eV.

ACKNOWLEDGMENTS

We are grateful to Dr. Emily Grumbling for experimental guidance and engaging discussions. This work was supported by the U.S. National Science Foundation (Grant No. CHE-1011895). L.M.C. acknowledges past support form the Arizona Science Foundation.

[1] B. H. Lipshutz, Chem. Rev. **86**, 795 (1986).
[2] O. S. L. Bruinsma, R. S. Geertsma, P. Bank, and J. A. Moulijn, Fuel **67**, 327 (1988).
[3] G. Schopf and G. Kossmehl, *Polythiophenes—Electrically Conductive Polymers* (Springer, Berlin, 1997), vol. 129, p. 3.
[4] M. Caironi, D. Natali, M. Sampietro, C. Bertarelli, A. Bianco, A. Dundulachi, E. Canesi, and G. Zerbi, Appl. Phys. Lett. **89**, 243519 (2006).
[5] A. Gandini, D. Coelho, M. Gomes, B. Reis, and A. Silvestre, J. Mater. Chem. **19**, 8656 (2009).
[6] M. H. Palmer, I. C. Walker, and M. F. Guest, Chem. Phys. **247**, 349 (1999).
[7] D. M. P. Holland, L. Karlsson, and W. von Niessen, J. Electron Spectrosc. Relat. Phenom. **113**, 221 (2001).

[8]E. E. Rennie, C. A. F. Johnson, J. E. Parker, D. M. P. Holland, D. A. Shaw, M. A. MacDonald, M. A. Hayes, and L. G. Shpinkova, Chem. Phys. **236**, 365 (1998).
[9]J. A. Sell and A. Kuppermann, Chem. Phys. Lett. **61**, 355 (1979).
[10]J. Yang, J. Li, and Y. X. Mo, J. Chem. Phys. **125**, 174313 (2006).
[11]H. A. Ho, H. Brisset, E. H. Elandaloussi, P. Frere, and J. Roncali, Adv. Mater. **8**, 990 (1996).
[12]S. Rentsch, J. P. Yang, W. Paa, E. Birckner, J. Schiedt, and R. Weinkauf, Phys. Chem. Chem. Phys. **1**, 1707 (1999).
[13]C. H. DePuy, S. R. Kass, and G. P. Bean, J. Org. Chem. **53**, 4427 (1988).
[14]K. M. Ervin and W. C. Lineberger, in *Advances in Gas Phase Ion Chemistry*, edited by N. G. Adams and L. M. Babcock (JAI Press, Greenwich, 1992), vol. 1, p. 121.
[15]K. M. Vogelhuber, S. W. Wren, L. Sheps, and W. C. Lineberger, J. Chem. Phys. **134**, 064302 (2011).
[16]E. Surber, R. Mabbs, and A. Sanov, J. Phys. Chem. A **107**, 8215 (2003).
[17]E. Surber, S. P. Ananthavel, and A. Sanov, J. Chem. Phys. **116**, 1920 (2002).
[18]A. Eppink and D. H. Parker, Rev. Sci. Instrum. **68**, 3477 (1997).
[19]D. W. Chandler and P. L. Houston, J. Chem. Phys. **87**, 1445 (1987).
[20]A. J. R. Heck and D. W. Chandler, Annu. Rev. Phys. Chem. **46**, 335 (1995).
[21]M. A. Johnson and W. C. Lineberger, in *Techniques for the Study of Ion Molecule Reactions*, edited by J. M. Farrar and W. H. Saunders (Wiley, New York, 1988), p. 591.
[22]W. C. Wiley and I. H. McLaren, Rev. Sci. Instrum. **26**, 1150 (1955).
[23]V. Dribinski, A. Ossadtchi, V. A. Mandelshtam, and H. Reisler, Rev. Sci. Instrum. **73**, 2634 (2002).
[24]C. N. Yang, Phys. Rev. **74**, 764 (1948).
[25]J. Cooper and R. N. Zare, J. Chem. Phys. **49**, 4252 (1968).
[26]M. J. Frisch, G. W. Trucks, H. B. Schlegel *et al.*, GAUSSIAN 09, Revision A.1, Gaussian, Inc., Wallingford, CT, 2009.
[27]E. P. Wigner, Phys. Rev. **73**, 1002 (1948).
[28]E. Surber and A. Sanov, J. Chem. Phys. **118**, 9192 (2003).
[29]A. Sanov and R. Mabbs, Int. Rev. Phys. Chem. **27**, 53 (2008).
[30]D. J. Goebbert, K. Pichugin, and A. Sanov, J. Chem. Phys. **131**, 164308 (2009).
[31]K. M. Ervin, W. Anusiewicz, P. Skurski, J. Simons, and W. C. Lineberger, J. Phys. Chem. A **107**, 8521 (2003).
[32]F. A. Akin, L. K. Schirra, and A. Sanov, J. Phys. Chem. A **110**, 8031 (2006).
[33]M. Van Duzor, F. Mbaiwa, J. Wei, T. Singh, R. Mabbs, A. Sanov, S. J. Cavanagh, S. T. Gibson, B. R. Lewis, and J. R. Gascooke, J. Chem. Phys. **133**, 174311 (2010).
[34]R. Mabbs, F. Mbaiwa, J. Wei, M. Van Duzor, S. T. Gibson, S. J. Cavanagh, and B. R. Lewis, Phys. Rev. A **82**, 011401 (2010).
[35]S. J. Blanksby and G. B. Ellison, Acc. Chem. Res. **36**, 255 (2003).
[36]J. E. Bartmess, in *NIST Chemistry WebBook, NIST Standard Reference Database Number 69*, edited by P. J. Linstrom and W. G. Mallard (National Institute of Standards and Technology, Gaithersburg, MD, 2010); see http://webbook.nist.gov (retrieved January 12, 2010).
[37]J. Berkowitz, G. B. Ellison, and D. Gutman, J. Phys. Chem. **98**, 2744 (1994).
[38]E. P. Clifford, P. G. Wenthold, W. C. Lineberger, G. B. Ellison, C. X. Wang, J. J. Grabowski, F. Villa, and K. D. Jordan, J. Chem. Soc., Perkin Trans. 2 **2**, 1015 (1998).
[39]R. F. Gunion, M. K. Gilles, M. L. Polak, and W. C. Lineberger, Int. J. Mass Spectrom. **117**, 601 (1992).
[40]C. Barckholtz, T. A. Barckholtz, and C. M. Hadad, J. Am. Chem. Soc. **121**, 491 (1999).
[41]When elucidating the effect of electron delocalization on radical stabilities, one should consider the orbitals of the neutral radicals themselves, rather than the anions. To this end, inspection of the half-filled HOMOs of $^{\bullet}C_4H_3S$ and $^{\bullet}C_4H_3O$ leads to the same qualitative conclusion as that presented in the text based on the anion orbitals.